

Variability of the
transport of
anthropogenic CO₂ at
the OVIDE section

P. Zunino et al.

Variability of the transport of anthropogenic CO₂ at the Greenland–Portugal OVIDE section: controlling mechanisms

P. Zunino¹, M. I. Garcia-Ibañez², P. Lherminier¹, H. Mercier³, A. F. Rios², and F. F. Pérez²

¹Ifremer, Laboratoire de Physique des Océans, UMR6523 CNRS/Ifremer/IRD/UBO, Ifremer Centre de Brest, CS 10070, Plouzané, France

²Instituto de Investigaciones Marinas, IIM-CSIC, 36208 Vigo, Spain

³CNRS, Laboratoire de Physique des Océans, UMR6523 CNRS/Ifremer/IRD/UBO, Ifremer Centre de Brest, CS 10070, Plouzané, France

Received: 9 September 2013 – Accepted: 4 October 2013 – Published: 18 October 2013

Correspondence to: P. Zunino (pzunino@ifremer.fr)

Published by Copernicus Publications on behalf of the European Geosciences Union.

Title Page

Abstract

Introduction

Conclusions

References

Tables

Figures

⏪

⏩

◀

▶

Back

Close

Full Screen / Esc

Printer-friendly Version

Interactive Discussion

Abstract

The interannual to decadal variability of the transport of anthropogenic carbon dioxide (Cant) across the Subpolar North Atlantic (SPNA) is investigated, using data of the OVIDE high resolution transoceanic section, from Greenland to Portugal, occupied six times from 1997 to 2010. The transport of Cant across this section, T_{Cant} hereafter, is northward, with a mean value of $254 \pm 29 \text{ kmols}^{-1}$ over the 1997–2010 period. The T_{Cant} presents a high interannual variability, masking any trend different from 0 for this period. In order to understand the mechanisms controlling the variability of the T_{Cant} across the SPNA, we propose a new method that quantifies the transport of Cant caused by the diapycnal and isopycnal circulation. The diapycnal component yields a large northward transport of Cant ($400 \pm 29 \text{ kmols}^{-1}$) which is partially compensated by a southward transport of Cant caused by the isopycnal component ($-171 \pm 11 \text{ kmols}^{-1}$), mainly localized in the Irminger Sea. Most importantly, the diapycnal component is found to be the main driver of the variability of the T_{Cant} across the SPNA. Both the Meridional Overturning Circulation (MOC) and the Cant increase in the water column have an important effect on the variability of the diapycnal component and of the T_{Cant} itself. Based on this analysis, we propose a simplified estimator for the variability of the T_{Cant} based on the intensity of the MOC and on the difference of Cant between the upper and lower limb of the MOC (ΔCant). This estimator shows a good consistency with the diapycnal component of the T_{Cant} , and help to disentangle the effect of the variability of both the circulation and the Cant increase on the T_{Cant} variability. We find that ΔCant keeps increasing over the past decade, and it is very likely that the continuous Cant increase in the water masses will cause an increase in the T_{Cant} across the SPNA at long time scale. Nevertheless, at the time scale analyzed here (1997–2010), the MOC is controlling the T_{Cant} variability, blurring the expected T_{Cant} increase. Extrapolating the observed ΔCant increase rate and considering the predicted slow-down of 25 % of the MOC, the T_{Cant} across the SPNA is expected to

Variability of the transport of anthropogenic CO₂ at the OVIDE section

P. Zunino et al.

Title Page

Abstract

Introduction

Conclusions

References

Tables

Figures



Back

Close

Full Screen / Esc

Printer-friendly Version

Interactive Discussion



increase by 430 kmols^{-1} during the 21st century. Consequently, an increase in the storage rate of Cant in the SPNA could be envisaged.

1 Introduction

The ocean acts as an important sink for the CO_2 emitted by human activities. It has stored approximately one-third of the total anthropogenic carbon dioxide (Cant hereafter) emissions since the beginning of the industrial era (Sabine et al., 2004). Cant is uptaken by the air–sea interface and its distribution depends on mixing processes and transport into the ocean interior, this is the reason why Cant generally decreases with increasing depth. The storage of Cant in the deep ocean depends on the ventilation and formation of intermediate and deep waters (Tanhua et al., 2006; Rhein et al., 2007; Steinfeldt et al., 2009).

Among all oceans, the highest rate of Cant storage is found in the North Atlantic, mainly in the subpolar region (Sabine et al., 2004; Khatiwala et al., 2013). An increase in Cant storage is associated with an increase in the Cant concentration of the water masses. The rate at which the Cant concentration increases in the different water masses depends on both their ages and their positions in the water column. In the subpolar North Atlantic (SPNA hereafter), the upper layers, Subantartic Intermediate Water (SAIW), Subpolar Mode Water (SPMW) and North Atlantic Central Water (NACW), present the highest Cant increase trends, changing from average values of $35\text{--}40 \mu\text{mol kg}^{-1}$ in 1991–1993 up to $55 \mu\text{mol kg}^{-1}$ in 2006 (Pérez et al., 2010). Besides, the production of Labrador Sea Water (LSW) fosters a fast injection of Cant in the intermediate and deep waters, so that, this water mass also presents a high trend of Cant increase. Otherwise, the deeper water masses of the Eastern North Atlantic show no significant tendencies in their Cant content between 1991 and 2006 (Pérez et al., 2010).

In the North Atlantic the highest air–sea fluxes of Cant are detected at mid-latitude (Mikaloff Fletcher et al., 2006). Besides, Pérez et al. (2013) have inferred that Cant

Variability of the transport of anthropogenic CO₂ at the OVIDE section

P. Zunino et al.

[Title Page](#)[Abstract](#)[Introduction](#)[Conclusions](#)[References](#)[Tables](#)[Figures](#)[⏪](#)[⏩](#)[◀](#)[▶](#)[Back](#)[Close](#)[Full Screen / Esc](#)[Printer-friendly Version](#)[Interactive Discussion](#)

is the main component of the air–sea CO₂ fluxes at mid-latitude in the North Atlantic while the natural component is the dominant one in the subpolar region. They also detected a decrease in the storage rate of Cant between 1997 and 2006 in the subpolar region that was related to the reduction of the intensity of the Meridional Overturning Circulation (MOC). Based on those findings, they elucidated the important contribution of the lateral advection of Cant from mid to high latitudes to the Cant storage in the SPNA. The other important element of the Cant storage in the SPNA is the advection of water masses recently ventilated such as the different vintages of Labrador Sea Water. Consequently, how Cant is transported in the SPNA is a crucial issue for understanding how the ocean is storing Cant and for modelling the future role of the ocean damping the atmospheric CO₂ increase caused by the mankind.

Nowadays, there is an important international effort in understanding how the ocean is uptaking, distributing and storing Cant. On the one hand, there are estimations of CO₂ fluxes computed from sea surface pCO₂ measurements, ocean inversion, atmospheric inversion and/or ocean biogeochemical models. On the other hand, some of these methods also provide estimation of transport of Cant (T_{Cant} hereafter) in the ocean (see Mikaloff Fletcher et al., 2006; Gruber et al., 2009; Tjiputra et al., 2010), but unfortunately, direct estimations of T_{Cant} are not abundant and they are concentrated in the Atlantic Ocean. In the North Atlantic, the T_{Cant} has been estimated from observational data across 24° N and across a transversal section between 40° N and 60° N. The T_{Cant} is larger at mid-latitude than in the northernmost section (see Table 1). There are large differences between the uncertainties given for the T_{Cant} estimations in Table 1. These differences are very likely due to the different methods used for computing the volume transport since most of the T_{Cant} errors come from the volume transport uncertainties. Comparing the observation-based T_{Cant} and the T_{Cant} estimated by ocean inversions or by biogeochemical models, the observation-based estimations are in general larger than the others (see Table 1). It evidences that further improvements in circulation models are necessary in order to provide more realistic T_{Cant} estimations from ocean inversions and biochemical models. To bridge the gap between observa-

tions and models, it is necessary to better understand what circulation mechanisms are controlling the T_{Cant} and its temporal variability. For example, following the results of Pérez et al. (2013), it seems crucial that models reproduce a realistic variability of the Atlantic Meridional Overturning Circulation.

5 In this work, in order to analyse the T_{Cant} variability across the SPNA, data measured between 1997 and 2010 from Greenland to Portugal (FOUREX and OVIDE sections, see Fig. 1) were used. The circulation across this section was described by Lherminier et al. (2007, 2010) and Mercier et al. (2013). Briefly, at gyre scale, the structures intersecting the section are: a cyclonic circulation in the Irminger Sea, a cyclonic circulation
10 in the Iceland Basin, the North Atlantic Current (NAC) flowing directly northward east of Eriador Seamount, and lastly, an anticyclonic circulation dominating the West European Basin. Beside this gyre-scale circulation, the MOC is an important feature of the circulation across the OVIDE section. It transports warm, Cant-laden surface water northward, mainly by the NAC. North of the section, waters are transformed in cold waters that are poorer in Cant and flow southwards close to Greenland, forming the Deep
15 Western Boundary Current (DWBC). The limit between the upper and lower limbs of the MOC has been defined by σ_1 (potential density referenced to 1000 dbar) equal to $32.14 \pm 0.03 \text{ kmol m}^{-3}$ (called σ_{MOC} , Mercier et al., 2013).

The MOC has been identified as the element of the circulation mainly driving the heat transport across several transoceanic sections in the North Atlantic meanwhile the horizontal or isopycnal transport has a minor impact (Ganachaud and Wunsch, 2003; Mercier et al., 2013). Recently, Pérez et al. (2013) have evaluated the T_{Cant} variability across the subpolar gyre finding a significant impact of the MOC on the T_{Cant} variability.
20

Following Pérez et al. (2013) and using a longer time series we want to go further. First, we evaluate for the first time the variability of the T_{Cant} across the SPNA at inter-
25 annual to decadal time scale. Second, we propose a new method in order to evaluate the effect of the different elements of the ocean circulation on the T_{Cant} variability. Third, we propose a simplified estimator for the T_{Cant} across the SPNA based on the factors chiefly responsible of its variability. Finally, we analyse the influence of the increase in

BGD

10, 16101–16135, 2013

Variability of the transport of anthropogenic CO₂ at the OVIDE section

P. Zunino et al.

Title Page

Abstract

Introduction

Conclusions

References

Tables

Figures

⏪

⏩

◀

▶

Back

Close

Full Screen / Esc

Printer-friendly Version

Interactive Discussion

Cant in the ocean in the T_{Cant} variability. The paper is organized as follows: data and the main water masses circulating across the OVIDE section are detailed in Sect. 2; the T_{Cant} computation as well as a new method to clarify the effect of the different component of the circulation on the T_{Cant} are explained in Sect. 3; the main results of this work are exposed in Sect. 4; finally, results are discussed in Sect. 5.

2 Data sets

The data used in the study were acquired during the FOUREX and OVIDE cruises (Table 2, Fig. 1), where full-depth hydrographic stations were carried out between Greenland and Portugal. An overview of the instruments and calibrations associated with the physical parameters is presented by Mercier et al. (2013) and summarized hereafter. The CTDO2 measurement accuracies are better than 1 dbar for pressure P , 0.002°C for temperature T , 0.003 for salinity S and $1\ \mu\text{mol kg}^{-1}$ for dissolved oxygen O_2 (Billant et al., 2004; Branellec and Thierry, 2013). The current velocities perpendicular to the section were estimated by combining the geostrophic currents and the velocities measured by the Vessel-Mounted Acoustic Doppler Current Profilers in an inverse model using the generalized least squares (Mercier, 1986; Lux et al., 2000). The specificities associated with the OVIDE section are detailed by Lherminier et al. (2007, 2010).

The measurements relative to the CO_2 system were all obtained from bottle samples. The pH was determined with a spectrophotometric method (Clayton and Byrne, 1993) resulting in an accuracy of 0.003 pH units or better. The total alkalinity (A_T) was analysed with potentiometric titration and determined by single point titration (Pérez and Fraga, 1987; Mintrop et al., 2002), with an accuracy of $4\ \mu\text{mol kg}^{-1}$. The total inorganic carbon (C_T) was calculated from pH and total A_T , following the recommendations and guidelines from Velo et al. (2010). Then, the concentration of anthropogenic carbon dioxide (Cant) is determined from C_T , A_T , oxygen, nutrients, T and S , applying the method ϕCt° (Pérez et al., 2008; Vázquez-Rodríguez et al., 2009). A random propaga-

BGD

10, 16101–16135, 2013

Variability of the transport of anthropogenic CO_2 at the OVIDE section

P. Zunino et al.

Title Page

Abstract

Introduction

Conclusions

References

Tables

Figures

⏪

⏩

◀

▶

Back

Close

Full Screen / Esc

Printer-friendly Version

Interactive Discussion

tion of the errors associated with the input variables yielded an overall uncertainty of $\pm 5.2 \mu\text{mol kg}^{-1}$ on the Cant concentration.

The vertical sections of properties (potential temperature (θ), S , Cant) are shown for 2002 and 2010 in Fig. 2. They show the gradient of surface properties from cold, fresh waters in the Irminger Sea to warm, salty and Cant-rich waters toward Portugal. The strongest surface fronts east of the Eriador Seamount (ESM) mark the branches of the North Atlantic Current (NAC, see Lherminier et al., 2010). Note however that the penetration of Cant in the first 1000 m is comparable in the Irminger Sea and in the Iberian Abyssal Plain.

At intermediate depth, the minimum of salinity marks the Labrador Sea Water (LSW) and is observed from the Greenland slope to the Azores–Biscay Rise. Following Yashayaev et al. (2007), we will distinguish two vintages of the LSW: the upper LSW (uLSW) also called LSW₂₀₀₀ ($32.32 < \sigma_1 < 32.37$) and the classical LSW (cLSW) also called LSW_{1987–1994} ($32.40 < \sigma_1 < 32.44$). Both classes of LSW are marked by a relative maximum in Cant, due to their recent ventilation in the Labrador Sea, although it is much less clear for the cLSW in 2010, consistently with the fact that this water mass was not ventilated between 1994 and 2008 (Yashayaev and Loder, 2009).

Deep and bottom waters below the LSW have very different properties in the SPNA and in the inter-gyre region. Northwest of the ESM, those waters are rich in overflow waters coming from the Nordic Sea: the Iceland–Scotland Overflow Water (ISOW, below cLSW) and the Denmark Strait Overflow Water (DSOW, below $\sigma_1 = 32.53 \text{ kg m}^{-3}$). Southeast of the ESM, the deep and bottom waters are rich in Antarctic Bottom Water (AABW), that has not been in contact with the atmosphere for several decades and presents a concentration in Cant close to $0 \mu\text{mol kg}^{-1}$. This distribution creates a horizontal gradient of Cant at the bottom, from Cant-free water in the southeast to relatively Cant-rich overflow water in the northwest.

Between 2002 and 2010, the concentration of Cant increased dramatically over the whole section, except in the AABW derived water where Cant concentration is very

BGD

10, 16101–16135, 2013

Variability of the transport of anthropogenic CO₂ at the OVIDE section

P. Zunino et al.

Title Page

Abstract

Introduction

Conclusions

References

Tables

Figures

⏪

⏩

◀

▶

Back

Close

Full Screen / Esc

Printer-friendly Version

Interactive Discussion

low. As we will see in the results, this increase has a big impact on the variability of the transport of Cant across the section.

All the trends given in this work were estimated fitting a straight line by means of least squares. Confidence intervals were calculated considering a T -student distribution at the 95 % confidence level. The mean values estimated for a period of time are given with the standard error, i.e. $\pm\sigma/\sqrt{N}$ where N is the number of data.

3 Method: transport of anthropogenic CO₂ and its decomposition

The transport of any property across the Greenland to Portugal section can be computed as:

$$T_{\text{prop}} = \int_{\text{Greenland}}^{\text{Portugal}} \int_{\text{bottom}}^{\text{surface}} v\rho[\text{Prop}]dx dz \quad (1)$$

where v is the velocity orthogonal to the section, ρ is the in situ density and $[\text{Prop}]$ is the concentration of any variable. Note that x is the horizontal coordinate along the section and z is the vertical coordinate. The error of the transport of any property is calculated in the inverse model using the co-variance matrix of errors (Lherminier et al., 2007).

Understanding the processes by which the ocean transports heat, freshwater and Cant is an important issue in climate modelling. In order to evaluate the elements of the circulation that influence the heat transport across transoceanic sections, several authors, for example Böning and Herrman (1994) or Bryden and Imawaki (2001), suggested the decomposition of heat transport into three parts. This methodology has been widely applied for both heat and salt fluxes in the majority of the oceans, but in the case of Cant, it has only been applied by Alvarez et al. (2003). Following the previous authors, for a transoceanic section velocity (V) and Cant can be split into three

Variability of the transport of anthropogenic CO₂ at the OVIDE section

P. Zunino et al.

Title Page

Abstract

Introduction

Conclusions

References

Tables

Figures

⏪

⏩

◀

▶

Back

Close

Full Screen / Esc

Printer-friendly Version

Interactive Discussion

components:

$$V(x, z) = V_0 + \langle v \rangle(z) + v'(x, z) \quad (2)$$

$$\text{Cant}(x, z) = \text{Cant}_0 + \langle \text{Cant} \rangle(z) + \text{Cant}'(x, z) \quad (3)$$

5 where V_0 and Cant_0 are the section-averaged values, $\langle v \rangle(z)$ and $\langle \text{Cant} \rangle(z)$ are the horizontal average profiles and $v'(x, z)$ and $\text{Cant}'(x, z)$ are the deviation from the horizontal average profiles. In the same way the transport of Cant (T_{Cant} , Eq. 1) can be decomposed in three components (Eq. 4) where the overbar denotes the area integration over the OVIDE section.

$$10 \quad T_{\text{Cant}} = \rho V_0 \text{Cant}_0 + \overline{\rho \langle v \rangle \langle \text{Cant} \rangle} + \overline{\rho v' \text{Cant}'} \quad (4)$$

Alvarez et al. (2003) carried out the decomposition of T_{Cant} across the FOUREX section (see Fig. 1) using pressure as vertical coordinate, the same way than heat and salt transport decompositions are usually done. Because of the strong horizontal density gradient and the general circulation across the section we think that across this section it is preferable to do the decomposition in density coordinate ($z = \sigma_1$). Indeed, along the OVIDE section, the upper and lower branches of the Meridional Overturning Circulation (MOC), namely, the northward North Atlantic Current (NAC) and the southward Western Boundary Current (WBC) respectively, overlap in the depth coordinate while they have distinct density properties. Therefore, when the transport is computed in pressure coordinate, the MOC intensity is underestimated (Lherminier et al., 2010; Mercier et al., 2013). Thus, we think that the T_{Cant} computation and decomposition should be done in density coordinate.

It is the very first time that the T_{Cant} decomposition exposed in Eq. (4) is computed in density coordinate. Respecting the order of the different terms, Eq. (4) can be written as:

$$25 \quad T_{\text{Cant}} = T_{\text{Cant}}^{\text{net}} + T_{\text{Cant}}^{\text{diap}} + T_{\text{Cant}}^{\text{isop}} \quad (5)$$

Variability of the transport of anthropogenic CO₂ at the OVIDE section

P. Zunino et al.

Title Page

Abstract

Introduction

Conclusions

References

Tables

Figures

◀

▶

◀

▶

Back

Close

Full Screen / Esc

Printer-friendly Version

Interactive Discussion



computed the T_{Cant} across the OVIDE section between 2002 and 2006 (cyan diamonds in Fig. 3), their mean value for that period is $195 \pm 24 \text{ kmols}^{-1}$. For the same period, we obtain a mean value of $208 \pm 40 \text{ kmols}^{-1}$, a compatible result considering the error bars.

Looking at the evolution of T_{Cant} between 1997 and 2010 (black line in Fig. 3), it presents a high interannual variability, showing a decrease from 1997 to 2006 and a recovery hereafter. Note that this T_{Cant} recovery and the significant highest value in 2010 ($380 \pm 64 \text{ kmols}^{-1}$) have never been published before. The trend for the whole period of time is $4.0 \pm 15.5 \text{ kmols}^{-1} \text{ yr}^{-1}$. This result is statistically not different from 0 since the interannual variability blurs the longer time scale variability, at least, over this 14 yr period of time.

4.2 Decomposition of the transport of anthropogenic CO_2 across the Greenland–Portugal section

The evolution of each of the diapycnal ($T_{\text{Cant}}^{\text{diap}}$), isopycnal ($T_{\text{Cant}}^{\text{isop}}$) and net ($T_{\text{Cant}}^{\text{net}}$) transport of Cant are also displayed in Fig. 3. The sum of these three components is exactly the total Cant flowing across the OVIDE section. The 1997–2010 mean value of $T_{\text{Cant}}^{\text{diap}}$, $T_{\text{Cant}}^{\text{isop}}$ and $T_{\text{Cant}}^{\text{net}}$ are $400 \pm 29 \text{ kmols}^{-1}$, $-171 \pm 11 \text{ kmols}^{-1}$ and $26 \pm 9 \text{ kmols}^{-1}$ respectively. For all the years, the $T_{\text{Cant}}^{\text{diap}}$ is larger than the T_{Cant} meanwhile the $T_{\text{Cant}}^{\text{isop}}$ is always negative. Finally, the net transport is the smallest contribution to the T_{Cant} since the net transport of volume across the section is very low, less than 1 Sv, and because the section average of Cant is around $26 \mu\text{mol kg}^{-1}$.

The $T_{\text{Cant}}^{\text{isop}}$ is the transport of Cant along isopycnals. It is the integration of the covariance of the anomalies of volume transport and Cant at each station and density level across the section. Note that these anomalies are the resultants of subtracting to each data profile the section average value (V_0 and Cant_0 , see Eqs. 2 and 3) and the section average profile ($\langle V \rangle(z)$ and $\langle \text{Cant} \rangle(z)$, see Eqs. 2–4). The $T_{\text{Cant}}^{\text{isop}}$ shows

BGD

10, 16101–16135, 2013

Variability of the transport of anthropogenic CO_2 at the OVIDE section

P. Zunino et al.

Title Page

Abstract

Introduction

Conclusions

References

Tables

Figures

⏪

⏩

◀

▶

Back

Close

Full Screen / Esc

Printer-friendly Version

Interactive Discussion

Variability of the transport of anthropogenic CO₂ at the OVIDE section

P. Zunino et al.

[Title Page](#)

[Abstract](#)

[Introduction](#)

[Conclusions](#)

[References](#)

[Tables](#)

[Figures](#)

[⏪](#)

[⏩](#)

[◀](#)

[▶](#)

[Back](#)

[Close](#)

[Full Screen / Esc](#)

[Printer-friendly Version](#)

[Interactive Discussion](#)

a no negligible southward transport of Cant across the OVIDE section. The result contrasts with the isopycnal transport of heat (Mercier et al., 2013) that has a minor contribution to the total heat flux in the North Atlantic (Ganachaud and Wunsch, 2003). In the following, we analyze the spatial distribution of the $T_{\text{Cant}}^{\text{isop}}$ to understand the origin of its southward resultant. Figure 4a displays the mean value of $T_{\text{Cant}}^{\text{isop}}$ over 1997–2010, accumulated from Greenland to Portugal and from the bottom to each density level. For water denser than 32.14 kg m^{-3} the accumulated $T_{\text{Cant}}^{\text{isop}}$ is -150 kmols^{-1} , which is the 87 % of the total (-171 kmols^{-1}). It points out that, for the whole section, the transport of Cant along isopycnals occurs mainly in the dense waters. To locate the main region contributing to the $T_{\text{Cant}}^{\text{isop}}$, the latter is vertically integrated and horizontally accumulated from Greenland to each station along the section (Fig. 4b). The maximum negative value is reached approximately at 200 km from Greenland, exactly where the maximum negative value of volume transport is found (Fig. 4c). From that point eastward, a northward transport of Cant caused by the recirculation in the Irminger Sea diminished the total southward $T_{\text{Cant}}^{\text{isop}}$ in this basin (Fig. 4b). In the intermediate and deep waters east of Reykjanes Ridge, anomalies of Cant in isopycnal layers are quite small resulting in a weak contribution to the $T_{\text{Cant}}^{\text{isop}}$, this is why the $T_{\text{Cant}}^{\text{isop}}$ in waters denser than 32.14 kg m^{-3} is almost constant eastward of the Iceland Basin (Fig. 4b). Instead, taking into account the whole water column, there is a southward $T_{\text{Cant}}^{\text{isop}}$ in the Western European Basin (WEB, Fig. 4b) mainly explained by a northward advection (Fig. 4c) of a negative anomaly of Cant in the surface layers. Indeed, on a given isopycnal in the Western European Basin (WEB) and the Iberian Abyssal Plain (IAP), the surface layers are less rich in Cant than in the Irminger Sea (Fig. 2). We can then conclude that southward transport of Cant associated with the isopycnal component is mainly occurring in the Irminger Sea. In order to identify the water masses mainly responsible of this transport, the transport of Cant associated with the isopycnal component is horizontally but not vertically integrated (Fig. 4d). Two different ranges of densities are identified as

Variability of the transport of anthropogenic CO₂ at the OVIDE section

P. Zunino et al.

[Title Page](#)

[Abstract](#)

[Introduction](#)

[Conclusions](#)

[References](#)

[Tables](#)

[Figures](#)

[⏪](#)

[⏩](#)

[◀](#)

[▶](#)

[Back](#)

[Close](#)

[Full Screen / Esc](#)

[Printer-friendly Version](#)

[Interactive Discussion](#)



the major contributions to the $T_{\text{Cant}}^{\text{isop}}$: the lower lobe ($32.48 < \sigma_1 < 32.55 \text{ kg m}^{-3}$) corresponds to the overflow waters (DSOW and ISOW), while the upper lobe corresponds to intermediate and surface waters of the Irminger Sea (note the shallow position of $\sigma_1 = 32.14 \text{ kg m}^{-3}$ in the Irminger Sea, Fig. 2). In this basin, the waters corresponding to the density range of both lobes contain high concentration of Cant (see Fig. 2) due to their recent formation and/or ventilation. To summarize, the southward resultant of $T_{\text{Cant}}^{\text{isop}}$ is mainly localized in the Irminger Sea where the southward transport of Cant caused by the Western Boundary Current (WBC) is partially compensated by the northward transport caused by the inner recirculation in this basin. Concerning water masses, only LSW has a minor contribution to the $T_{\text{Cant}}^{\text{isop}}$ that is further discussed in Sect. 5.

The transport of Cant across isopycnals, that is the $T_{\text{Cant}}^{\text{diap}}$, is decomposed in terms of anomalies of volume transport (Fig. 5a) and anomalies of Cant concentration (Fig. 5b) computed in isopycnal layers (with a resolution of 0.01 kg m^{-3}). As explained in the method section, for this component, anomalies are computed from section-average values. The MOC upper and lower limbs can be identified in Fig. 5a, with northward (southward) volume transports above (below) σ_{MOC} . In the upper limb, the Cant-laden surface water transported northward by the NAC results in a positive $T_{\text{Cant}}^{\text{diap}}$ (Fig. 5c). In the densest waters ($\sigma_1 > 32.4$), both transport and Cant anomalies are negative (Fig. 5a and b); the former because the lower limb of the MOC flows southwards and the latter because deep waters are poorer in Cant than the average. As a result, the $T_{\text{Cant}}^{\text{diap}}$ is also positive in the densest layers (Fig. 5c). Looking in more details, it could be surprising to see such a positive peak in the overflow-derived water (waters denser than 32.40 kg m^{-3} in Fig. 5c). As a matter of fact, those deep and bottom waters are quite diluted when arriving at 60° N because of the entrainment of surrounding water poor in Cant on their way (Lherminier et al., 2010), so that their average concentration in Cant is actually smaller than the average over the whole section, resulting in a negative Cant anomaly (Fig. 5b). Once combined with the very strong southward transport (Fig. 5a),

this anomaly results in a positive peak of a similar intensity than the NAC contribution, but over a much thinner layer. To summarize, both surface and deep contributions sum up to a strongly positive $T_{\text{Cant}}^{\text{diap}}$ once integrated vertically.

4.3 Variability of the transport of Cant

In this part of the paper the T_{Cant} variability across the OVIDE section is analyzed. We expect that changes of both circulation and Cant concentration of the water masses have certain influence on the T_{Cant} variability. In the previous section we have separated the T_{Cant} caused by two different elements of the ocean circulation. In this section we are going to evaluate which elements of the circulation have a major influence in the T_{Cant} variability and whether the Cant increase in the water masses affects the T_{Cant} variability.

4.3.1 Variability of the components of the T_{Cant}

It is observed that the variability of the T_{Cant} and the $T_{\text{Cant}}^{\text{diap}}$ (black and blue lines in Fig. 3) are very well correlated ($r = 0.99$, p value = 0.0002). By contrast, the $T_{\text{Cant}}^{\text{isop}}$ presents a small variability that is not correlated with T_{Cant} ($r = -0.44$, p value = 0.38), and the same is true for the $T_{\text{Cant}}^{\text{net}}$ ($r = 0.40$, p value = 0.43). From here we can say that the diapycnal component is mainly driving the variability of the T_{Cant} .

In terms of volume transport, the diapycnal component is directly related to the MOC. Perez et al. (2013) suggested that the weakening of the lateral advection of Cant between 1997 and 2006, caused by the slow-down of the MOC, is the responsible of the decrease of the Cant storage rate during that period. However, during the period of time studied in this work (1997–2010), the MOC intensity (Fig. 6a) is correlated neither with the T_{Cant} ($r = 0.58$, p value = 0.23), nor with the $T_{\text{Cant}}^{\text{diap}}$ ($r = 0.68$, p value = 0.13). These results suggest that, although the diapycnal circulation is related to the MOC, in the case of the T_{Cant} , there is other factor acting on the $T_{\text{Cant}}^{\text{diap}}$ variability. It is very likely

Variability of the transport of anthropogenic CO₂ at the OVIDE section

P. Zunino et al.

Title Page

Abstract

Introduction

Conclusions

References

Tables

Figures

⏪

⏩

◀

▶

Back

Close

Full Screen / Esc

Printer-friendly Version

Interactive Discussion



that the Cant concentration change is the other factor controlling the variability of the $T_{\text{Cant}}^{\text{diap}}$ and so, the variability of the T_{Cant} .

4.3.2 A simplified estimator for the variability of the transport of Cant

The overturning circulation has been identified as the component of the circulation mainly driving the heat flux variability across the subpolar gyre (Mercier et al., 2013). After defining the MOC_{σ} as the maximum of the transport streamfunction, these authors approximated the heat transport variability across the OVIDE section taking into account the temperature difference between the upper limb and lower limb of the MOC_{σ} and the intensity of the latter. This method applied to the T_{Cant} could help us to clarify the effect of both circulation changes and Cant increase on the T_{Cant} variability. So, we propose the following estimator:

$$T_{\text{Cant}}^{\circ} = \Delta\text{Cant} \cdot \rho \cdot \text{MOC}_{\sigma} \quad (6)$$

where ΔCant is the difference between the mean value of Cant in the upper and lower limbs of the MOC_{σ} , ρ is the in situ density and MOC_{σ} is the intensity of the MOC computed in density coordinates. The time evolution of MOC_{σ} and ΔCant are showed in Fig. 6a.

We expect this estimator T_{Cant}° to be a good approximation of the $T_{\text{Cant}}^{\text{diap}}$ because it is taking into account the diapycnal circulation via the MOC intensity and not the isopycnal component of the circulation. Furthermore, by using the difference of Cant concentration between both limbs of the MOC, we are considering the Cant increase of waters flowing through the OVIDE section since we expect it has an important role in the $T_{\text{Cant}}^{\text{diap}}$ variability. As a matter of fact, the estimator T_{Cant}° is quite similar to the $T_{\text{Cant}}^{\text{diap}}$ (blue and cyan lines in Fig. 6b) and they are well correlated ($r = 0.82$, p value = 0.04).

To compare their variability, the anomalies of T_{Cant} , $T_{\text{Cant}}^{\text{diap}}$, and T_{Cant}° time series are plotted in Fig. 6c. Although we see by eye similar patterns between T_{Cant} and T_{Cant}°

BGD

10, 16101–16135, 2013

Variability of the transport of anthropogenic CO₂ at the OVIDE section

P. Zunino et al.

Title Page

Abstract

Introduction

Conclusions

References

Tables

Figures

◀

▶

◀

▶

Back

Close

Full Screen / Esc

Printer-friendly Version

Interactive Discussion



anomalies, the correlation ($r = 0.75$, p value = 0.09), is not as good as between $T_{\text{Cant}}^{\text{diap}}$ and T_{Cant}° since the estimator is not considering the isopycnal contribution.

As conclusion, the T_{Cant} cannot be totally inferred from the proposed estimator (T_{Cant}°) since the isopycnal component has a non-negligible contribution. Nevertheless, it is a good estimation of the $T_{\text{Cant}}^{\text{diap}}$, and, as the latter is mainly driving the T_{Cant} variability across the OVIDE section, this estimator is, at least, a pretty good indicator of the variability of the T_{Cant} across the section. Moreover, it will help us to disentangle the relative contribution of the circulation and the Cant increase in the variability of the T_{Cant} .

4.3.3 The effect of Cant concentration changes on the variability of the transport of Cant

In the OVIDE section during the period 1997–2010, the section-average Cant has increased at a rate of $0.29 \pm 0.21 \mu\text{mol kg}^{-1} \text{yr}^{-1}$, which means an increase of $4 \mu\text{mol kg}^{-1}$ between 1997 and 2010. The Cant increase of the upper limb of the MOC, that imports Cant into the subpolar region, is larger than the increase in the lower limb, which exports Cant from the subpolar region: $0.63 \pm 0.27 \mu\text{mol kg}^{-1} \text{yr}^{-1}$ and $0.20 \pm 0.25 \mu\text{mol kg}^{-1} \text{yr}^{-1}$ respectively, see Fig. 7.

In the previous section we presented an estimator, T_{Cant}° , which is a good indicator of the T_{Cant} variability across the OVIDE section. Using this estimator, if a steady circulation hypothesis is considered (MOC_{σ} constant, e.g. 16 Sv), the T_{Cant} increases at a rate of $7.0 \pm 1.6 \text{ kmols}^{-1} \text{yr}^{-1}$. It means that the Cant increase of the ocean waters yields an increase in the northward transport of Cant across the OVIDE section. However, the overturning circulation has an important role in the T_{Cant} variability, and it introduces a larger variability than the Cant increase at the interannual time scale. This is why the “real” trend estimated for the T_{Cant} for the period 1997–2010 is positive but not statistically different from 0.

Variability of the transport of anthropogenic CO₂ at the OVIDE section

P. Zunino et al.

Title Page

Abstract

Introduction

Conclusions

References

Tables

Figures

⏪

⏩

◀

▶

Back

Close

Full Screen / Esc

Printer-friendly Version

Interactive Discussion



Variability of the transport of anthropogenic CO₂ at the OVIDE section

P. Zunino et al.

Title Page

Abstract

Introduction

Conclusions

References

Tables

Figures

⏪

⏩

◀

▶

Back

Close

Full Screen / Esc

Printer-friendly Version

Interactive Discussion

To assess the relative role of the Cant concentration and circulation in the T_{Cant} and to compare with the analysis of Pérez et al. (2013), we choose to study the period between 1997 and 2006. During that period, the MOC intensity across the OVIDE section decreased (Mercier et al., 2013) at a rate of $-0.68 \pm 0.65 \text{ Sv yr}^{-1}$. Simultaneously, the T_{Cant} decreased at a rate of $-9.3 \pm 11.7 \text{ kmols}^{-1} \text{ yr}^{-1}$, while the Cant concentration increased at a rate of $0.48 \pm 0.56 \mu\text{mol kg}^{-1} \text{ yr}^{-1}$ and $0.01 \pm 0.42 \mu\text{mol kg}^{-1} \text{ yr}^{-1}$ in the upper and lower limbs of the MOC respectively. All these trends are not statistically different from 0 likely due to the low number of data, only 4, but they give insights that Cant increased in the upper limb of the MOC, meanwhile it hardly changed in the lower limb. Taking into account these results we conclude that, in the period between 1997 and 2006 the MOC decrease prevailed on the T_{Cant} variability. Indeed, using the proposed estimator (T_{Cant}°), if a steady circulation was considered, the T_{Cant} would increase at a rate of $7.8 \pm 3.2 \text{ kmols}^{-1} \text{ yr}^{-1}$ during the period 1997–2006. However, if Cant is maintained constant between 1997 and 2006, the T_{Cant} would decrease at a rate of $-15.3 \pm 14.6 \text{ kmols}^{-1} \text{ yr}^{-1}$, that is, the slow-down of the MOC would cause a decrease in the T_{Cant} statistically different from 0.

Over the whole studied period, 1997–2010, we found that the trends in T_{Cant} and T_{Cant}° are not significant. In the hypothetical case of a steady circulation, T_{Cant}° increases at a rate of $7.0 \pm 1.6 \text{ kmols}^{-1} \text{ yr}^{-1}$ since ΔCant is continuously increasing. Conversely, if ΔCant remains constant, T_{Cant}° variability follows the MOC variability with no trend.

All these results suggest that, at interannual to decadal time scale, the variability of the MOC is mainly driving the T_{Cant} variability across the OVIDE section. Nonetheless, the Cant increase is also causing a long term increase in the T_{Cant} that, at the time scale analyzed here, is being blurred by the interannual variability caused by the MOC variability.

5 Discussion and conclusions

The continuous increase of CO₂ concentration in the atmosphere due to human activities is being softened by the oceanic CO₂ uptake. The question is how long the ocean will act as a sink for this greenhouse gas. Therefore, it is really important to quantify and understand the mechanisms acting in its transport and storage in the oceans. It is well known that the North Atlantic presents the highest storage rate of Cant of the global oceans, mainly in the SPNA (Sabine et al., 2004). Recently, it has been demonstrated that the lateral advection provides the main supply of Cant to the SPNA (Pérez et al., 2013). In the last decade, the estimations of T_{Cant} by observational data and models yield quite different results: models tend to show lower values than data (Table 1). In this work we have focused in the physical aspect of the transport of Cant in order to understand the mechanisms driving the T_{Cant} across the SPNA and to describe for the first time its interannual to decadal variability.

In agreement with previous works (Alvarez et al., 2003; Pérez et al., 2013), we obtained a northward T_{Cant} across the OVIDE section. The mean value for the period 1997–2010 is $254 \pm 29 \text{ kmols}^{-1}$. The standard deviation of the T_{Cant} over the whole period, 71 kmols^{-1} , is larger than the error on each estimate, $\pm 48 \text{ kmols}^{-1}$, so the variability presented in Sect. 4.2 and discussed hereafter is meaningful. No significant long term changes have been identified during this period since the interannual variability is dominating (see black line in Fig. 3).

Splitting the T_{Cant} into its different components, we have observed that the isopycnal component causes a no negligible southward transport (see Fig. 3), mainly localized in the Irminger Sea (see Fig. 4). It contrasts with the heat fluxes across the North Atlantic Ocean, for which the isopycnal component has a minor contribution to the total heat flux (Ganachaud and Wunsch, 2003); across the OVIDE section specifically, the isopycnal heat flux accounts for less than 10 % of the total heat flux (Mercier et al., 2013). The different behaviour between T_{Cant} and heat fluxes across the OVIDE section is due to the differences in the horizontal gradient of Cant and temperature: Cant markedly

Variability of the transport of anthropogenic CO₂ at the OVIDE section

P. Zunino et al.

Title Page

Abstract

Introduction

Conclusions

References

Tables

Figures



Back

Close

Full Screen / Esc

Printer-friendly Version

Interactive Discussion



decreases eastward due to the age of the water masses, meanwhile the temperature presents a subtle increase (see Fig. 2). As a result, high positive anomalies of Cant are found in the Irminger Sea while the temperature anomalies are close to 0 °C. Therefore, the isopycnal contribution is more important in the $T_{\text{Cant}}^{\text{isop}}$ than in the heat flux.

To go further in the analysis of the isopycnal transport of Cant in the Irminger Sea, we found that the overflow waters (DSOW and ISOW) and intermediate and surface waters are mainly responsible for the southward transport (Fig. 4d). The fact that intermediate and surface waters of the Irminger Sea have a high contribution to the $T_{\text{Cant}}^{\text{isop}}$ is because its high Cant concentration as compared to the waters with the same density range in the WEB and IAP as for example Mediterranean Water (see Fig. 2). The high Cant content in the Irminger Sea is likely due to the recent ventilation of these waters, supporting the idea that deep convection in the Irminger Sea (Bacon et al., 2003; Pickart et al., 2003) reached depths down to 1000–1500 m in the 2000s. Vage et al. (2009) observed a 700 m-deep mixed layer in winter 2007–2008 for example. In the case of the overflow waters, the relatively high Cant concentration is mainly due to the entrainment of Cant-rich thermocline water at the sills during the process of overflow (Sarafanov et al., 2010).

Once identified the waters mainly responsible of the $T_{\text{Cant}}^{\text{isop}}$, the question is: why does the LSW, both upper and classical, yield a minor contribution to the $T_{\text{Cant}}^{\text{isop}}$ (see Fig. 4)? The answer is likely related to changes in the formation rate of these water masses and their spreading all along the OVIDE section. On the one hand, during the first half of the 90s, cLSW was abundantly formed in the Labrador Sea (Rhein et al., 2002), so it was enriched in Cant. In the mid-90s there was a shut-down in the formation of this water mass which was compensated by an enhanced production of uLSW in the Labrador Sea and possibly in the Irminger Sea (Yashayaev et al., 2007; Kieke et al., 2007; Rhein et al., 2011). Thenceforth, cLSW was exported to the Irminger Sea and northeast Atlantic taking between 6 months (Sy et al., 1997) to 2 yr (Straneo et al., 2003) to reach the Irminger Sea and 3–6 yr to get to the Mid-Atlantic Ridge (Kieke et al., 2009). Because of this spreading, cLSW was homogenized all along the

BGD

10, 16101–16135, 2013

Variability of the transport of anthropogenic CO₂ at the OVIDE section

P. Zunino et al.

Title Page

Abstract

Introduction

Conclusions

References

Tables

Figures

⏪

⏩

◀

▶

Back

Close

Full Screen / Esc

Printer-friendly Version

Interactive Discussion

OVIDE section, resulting in small Cant anomalies. On the other hand, the evolution of $T_{\text{Cant}}^{\text{isop}}$ in the uLSW density range during the period 1997–2010 displays more temporal variability (not shown), probably due to the intermittent ventilation of this water mass over the 2000s and to the advection timescales that are comparable to those of the cLSW. However, the average of $T_{\text{Cant}}^{\text{isop}}$ in the density range of uLSW for the 1997–2010 period is close to zero, this is why we identify a minor contribution of uLSW to the $T_{\text{Cant}}^{\text{isop}}$, and a more detailed analysis of its variability is out of the scope of this study.

The decomposition of the T_{Cant} shows also that the overturning component ($T_{\text{Cant}}^{\text{diap}}$) is the major contribution to the T_{Cant} , which mean value over the period 1997–2010 is $400 \pm 29 \text{ kmol s}^{-1}$. Moreover, as in the case of heat flux, it drives the variability of the T_{Cant} . The $T_{\text{Cant}}^{\text{diap}}$ is related to the MOC that transports warm and enriched Cant waters northward in its upper limb and denser, colder and poorer in Cant waters southward in its lower limb. The estimator T_{Cant}° is a schematic representation of this mechanism and indeed we found a good correlation between T_{Cant}° and $T_{\text{Cant}}^{\text{diap}}$. It also offers a simple proxy for testing numerical models. However, we are aware that T_{Cant}° does not represent all the processes involved in the transport of Cant in the SPNA.

To get an order of magnitude of the relative importance at long time scale of the Cant content and of the circulation on the T_{Cant} across the SPNA, we use T_{Cant}° . On the one hand, Cant is increasing faster in the upper limb of the MOC than in the lower limb, showing trends of $0.63 \pm 0.27 \mu\text{mol kg}^{-1} \text{ yr}^{-1}$ and $0.20 \pm 0.25 \mu\text{mol kg}^{-1} \text{ yr}^{-1}$ respectively during the period 1997–2010. It means that, in the SPNA, there is more Cant being imported in the upper limb than being exported in the lower limb, resulting in an accumulation of Cant in the SPNA, in agreement with Sabine et al. (2004) and Pérez et al. (2010). The minor increase of Cant in the lower limb is due to the dilution of the convected and overflow waters rich in Cant with the deep waters poor in Cant. We expect that the Cant concentration in both limbs is linked to the MOC variability, although we do not know at which time scale. Indeed, it depends on the advection of water from

BGD

10, 16101–16135, 2013

Variability of the transport of anthropogenic CO₂ at the OVIDE section

P. Zunino et al.

Title Page

Abstract

Introduction

Conclusions

References

Tables

Figures

⏪

⏩

◀

▶

Back

Close

Full Screen / Esc

Printer-friendly Version

Interactive Discussion

Variability of the transport of anthropogenic CO₂ at the OVIDE section

P. Zunino et al.

[Title Page](#)

[Abstract](#)

[Introduction](#)

[Conclusions](#)

[References](#)

[Tables](#)

[Figures](#)

[⏪](#)

[⏩](#)

[◀](#)

[▶](#)

[Back](#)

[Close](#)

[Full Screen / Esc](#)

[Printer-friendly Version](#)

[Interactive Discussion](#)

the subtropical areas in the upper limb, and on the processes of deep and intermediate water formation in the lower limb. However, it is striking that ΔC_{ant} keeps increasing independently of the MOC variability at a mean rate of $0.43 \pm 0.10 \mu\text{mol kg}^{-1} \text{yr}^{-1}$ (see pink line in Fig. 6a). This increasing rate is going to cause an augmentation in the T_{Cant} across the OVIDE section, and consequently, an increase in the storage rate in the SPNA. On the other hand, models have predicted a slow-down of 25 % of the MOC at the end of the present century (IPCC, 2007) independently of the interannual to decadal variability observed by Mercier et al. (2013). Taking into account the predicted slow-down of the MOC and the positive trend of ΔC_{ant} computed in this work, T_{Cant}° would increase at a rate of $4.3 \pm 0.1 \text{ kmols}^{-1} \text{yr}^{-1}$ during the 21st century. It means an increase of 430 kmols^{-1} of the T_{Cant} in 100 yr, despite the predicted slow-down of the MOC. To conclude, the faster increase of Cant in the upper limb than in the lower limb will cause an augmentation of the northward T_{Cant} across the SPNA at long time scale. Nevertheless, at the time scale analyzed in this work (1997–2010), the inter-annual variability of the MOC blurs the long term increase of the T_{Cant} caused by the ΔC_{ant} increase. Furthermore, this result is quite speculative since (i) we suppose that the trend in ΔC_{ant} will remain constant and (ii) we rely on the models for the decrease of the MOC. However, it gives an interesting order of magnitude.

We suspect that the long term increase of the T_{Cant} would cause an increase in the storage rate of Cant in the SPNA. Pérez et al. (2013) observed a decrease in the storage rate of Cant in the SPNA between 1997 (high MOC) and 2002–2006 (low MOC). They reported a change in the storage rate from $0.083 \pm 0.008 \text{ GtCyr}^{-1}$ to $0.026 \pm 0.004 \text{ GtCyr}^{-1}$ between both periods. However, because of the short time span, the ΔC_{ant} increase was too small to compensate for the large intra-decadal decrease in the MOC that caused the decrease in the T_{Cant} across the OVIDE section and consequently the decrease in the Cant storage rate reported by Pérez et al. (2013). Calculating the storage rate for 1997–2010 is the subject of a future work.

To sum up, although the isopycnal transport has a considerable contribution to the T_{Cant} across the OVIDE section, the major contribution to the T_{Cant} is the diapycnal

component which is also the main driver of its variability. In both components of the transport, the Cant concentration plays an important role: the horizontal gradient of Cant across the section is responsible for the southward transport of Cant by the isopycnal component while the northward transport of Cant-laden waters together with the southward transport of very poor in Cant waters are responsible for the large northward transport of Cant by the diapycnal component. Finally, we have shown that the variability of the MOC is dominating the variability of the T_{Cant} at interannual to decadal scale, but the Cant increase seems to control the T_{Cant} change at longer time scales. Therefore, in spite of the predicted slow-down of the MOC by 2100, an increase of the storage rate of Cant in the SPNA would be expected.

Acknowledgements. We are grateful to the captains, staff and researchers who contributed to the acquisition and processing of hydrographic data. The research leading to these results was supported through the EU FP7 project CARBOCHANGE “Changes in carbon uptake and emissions by oceans in a changing climate”, which received funding from the European Commission’s Seventh Framework Programme under grant agreement no. 264879. For this work P. Zunino was supported by the former project and by the Ifremer postdoctoral program. M. I. Garcia-Ibáñez was supported by the Spanish Ministry of Economy and Competitiveness (BES-2011-045614) through the CATARINA project (CTM2010-17141) co-funded by the Fondo Europeo de Desarrollo Regional 2007–2012 (FEDER). P. Lherminier was supported by the French Institute for Marine Science (Ifremer), H. Mercier by the French National Center for Scientific Research (CNRS), and A. F. Rios and F. F. Pérez by the Consejo Superior de Investigaciones Científicas (CSIC).



The publication of this article is financed by CNRS-INSU.

16122

BGD

10, 16101–16135, 2013

Variability of the transport of anthropogenic CO₂ at the OVIDE section

P. Zunino et al.

Title Page

Abstract

Introduction

Conclusions

References

Tables

Figures

⏪

⏩

◀

▶

Back

Close

Full Screen / Esc

Printer-friendly Version

Interactive Discussion



References

- Alvarez, M., Rios, A. F., Pérez, F. F., Bryden, H. L., and Roson, G.: Transports and budgets of total inorganic carbon in the subpolar and temperate North Atlantic, *Global Biogeochem. Cy.*, 17, 1002, doi:10.1029/2002GB001881, 2003.
- 5 Bacon, S., Gould, W. J., and Jia, Y.: Open-ocean convection in the Irminger Sea, *Geoph. Res. Lett.*, 30, 1246, doi:10.1029/2002GL016271, 2003.
- Billant, A., Branellec, P., and Mercier, H.: Campagne OVIDE 2002: Rapport de Données CTD-O₂, Tech. Rep. DRO/DOPS/04-01, 2004.
- 10 Böning, C. W. and Herrmann, P.: Annual cycle of poleward heat transport in the ocean: results from high-resolution modeling of the north and equatorial Atlantic, *J. Phys. Oceanogr.*, 24, 91–107, 1994.
- Branellec, P. and Thierry, V.: Campagne OVIDE 2010: Rapport de Données CTDO₂, Tech. Rep. ODE/OPS/LPO/13-01, 2013.
- Bryden, H. and Imawaki, S.: Ocean heat transport, in: *Ocean Circulation and Climate*, edited by: Siedler, G., Church, J., and Gould, J., Academic Press, 2001.
- 15 Clayton, T. D. and Byrne, R. H.: Calibration of m-cresol purple on the total hydrogen ion concentration scale and its application to CO₂-system characteristics in seawater, *Deep-Sea Res. Pt. I.*, 40, 2115–2129, 1993.
- Ganachaud, A. and Wunsch, C.: Large-scale ocean heat and freshwater transports during the World Ocean Circulation Experiment, *J. Climate*, 16, 696–705, 2003.
- 20 Gourcuff, C., Lherminier, P., Mercier, H., and Le Traon, P. Y.: Altimetry combined with hydrography for ocean transport estimation, *J. Atmos. Ocean Tech.*, 28, 1324–1337, doi:10.1175/2011JTECHO818.1, 2011.
- Grist, J. P., Marsh, R., and Josey, S. A.: On the relationship between the North Atlantic meridional overturning circulation and the surface-forced overturning streamfunction, *J. Climate.*, 22, 4989–5002, doi:10.1175/2009JCLI2574.1, 2009.
- 25 Gruber, N., Gloor, M., Mikaloff Fletcher, S. E., Doney, S. C., Dutkiewicz, S., Follows, M. J., Gerber, M., Jacobson, A. R., Joos, F., Lindsay, K., Menemenlis, D., Mouchet, A., Müller, S. A., Sarmiento, J. L., and Takahashi, T.: Oceanic sources, sinks, and transport of atmospheric CO₂, *Global Biogeochem. Cy.*, 23, GB1005, doi:10.1029/2008GB003349, 2009.
- 30 IPCC – Intergovernmental Panel on Climate Change: *Climate Change 2007: The Physical Science Basis*. Contribution of Working Group I to the Fourth Assessment Report of Intergov-

Variability of the transport of anthropogenic CO₂ at the OVIDE section

P. Zunino et al.

Title Page

Abstract

Introduction

Conclusions

References

Tables

Figures

⏪

⏩

◀

▶

Back

Close

Full Screen / Esc

Printer-friendly Version

Interactive Discussion



Variability of the transport of anthropogenic CO₂ at the OVIDE section

P. Zunino et al.

[Title Page](#)

[Abstract](#)

[Introduction](#)

[Conclusions](#)

[References](#)

[Tables](#)

[Figures](#)

[⏪](#)

[⏩](#)

[◀](#)

[▶](#)

[Back](#)

[Close](#)

[Full Screen / Esc](#)

[Printer-friendly Version](#)

[Interactive Discussion](#)

ernmental Panel on Climate Change, edited by: Solomon, S., Qin, D., Manning, M., Chen, Z., Marquis, M., Averyt, K. B., Tignorand, M., and Miller, H. L., Cambridge University Press, Cambridge, United Kingdom and New-York, NY, USA, 2007.

5 Khatiwala, S., Tanhua, T., Mikaloff Fletcher, S., Gerber, M., Doney, S. C., Graven, H. D., Gruber, N., McKinley, G. A., Murata, A., Ríos, A. F., and Sabine, C. L.: Global ocean storage of anthropogenic carbon, *Biogeosciences*, 10, 2169–2191, doi:10.5194/bg-10-2169-2013, 2013.

10 Kieke, D., Rhein, M., Stramma, L., Smethie, W. M., Bullister, J. L., and LeBel, D. A.: Changes in the pool of Labrador Sea Water in the subpolar North Atlantic, *Geoph. Res. Lett.*, 34, L06605, doi:10.1029/2006GL028959, 2007.

Kieke, D., Klein, B., Strammac, L., Rhein, M., and Koltermann, K. P.: Variability and propagation of Labrador Sea Water in the southern subpolar North Atlantic, *Deep-Sea Res. Pt. I*, 56, 1656–1674, doi:10.1016/j.dsr.2009.05.010, 2009.

15 Lherminier, P., Mercier, H., Gourcuff, C., Alvarez, M., Bacon, S., and Kermabon, C.: Transports across the 2002 Greenland–Portugal Ovide section and comparison with 1997, *J. Geophys. Res.*, 112, C07003, doi:10.1029/2006JC003716, 2007.

Lherminier, P., Mercier, H., Huck, T., Gourcuff, C., Perez, F. F., Morin, P., Sarafanov, A., and Falina, A.: The Atlantic Meridional Overturning Circulation and the subpolar gyre observed at the A25-OVIDE section in June 2002 and 2004, *Deep-Sea. Res. Pt. I*, 57, 1374–1391, doi:10.1016/j.dsr.2010.07.009, 2010.

20 Lux, M., Mercier, H., and Arhan, M.: Interhemispheric exchanges of mass and heat in the Atlantic Ocean in January–March 1993, *Deep-Sea Res. Pt. I*, 48, 605–638, 2000.

25 Macdonald, A. M., Baringer, M. O., Wanninkhof, R., Lee, K., and Wallace, D. W. R.: A 1998–1992 comparison of inorganic carbon and its transport across 24.51° N in the Atlantic, *Deep-Sea Res. Pt. II*, 50, 3041–3064, 2003.

Mercier, H.: Determining the general circulation of the ocean: a non linear inverse problem, *J. Geophys. Res.*, 91, 5103–5109, 1986.

30 Mercier, M., Lherminier, P., Sarafanov, A., Gaillard, F., Daniault, N., Desbroyères D., Falina, A., Ferron, B., Gourcuff, C., Huck, T., and Thierry, V.: Variability of the meridional overturning circulation at the Greenland–Portugal OVIDE section from 1993 to 2010, *Prog. Oceanogr.*, in press, 2013.

Mikaloff-Fletcher, S. E., Gruber, N., Jacobson, A. R., Doney, S. C., Dutkiewicz, S., Gerber, M., Follows, M., Joos, F., Lindsay, K., Menemenlis, D., Mouchet, A., Müller, S. A., and

Variability of the transport of anthropogenic CO₂ at the OVIDE section

P. Zunino et al.

[Title Page](#)

[Abstract](#)

[Introduction](#)

[Conclusions](#)

[References](#)

[Tables](#)

[Figures](#)

[⏪](#)

[⏩](#)

[◀](#)

[▶](#)

[Back](#)

[Close](#)

[Full Screen / Esc](#)

[Printer-friendly Version](#)

[Interactive Discussion](#)



- Sarmiento, J. L.: Inverse estimates of anthropogenic CO₂ uptake, transport, and storage by the ocean, *Global Biogeochem. Cy.*, 20, GB2002, doi:10.1029/2005GB002530, 2006.
- Mintrop, L., Pérez, F. F., Gonzalez-Davila, M., Santana-Casiano, M. J., and Kortzinger, A.: Alkalinity determination by potentiometry: intercalibration using three different methods, *Cienc. Mar.*, 26, 23–37, 2002.
- Pérez, F. F. and Fraga, F.: A precise and rapid analytical procedure for alkalinity determination, *Mar. Chem.*, 21, 169–182, 1987.
- Pérez, F. F., Vazquez-Rodríguez, M., Louarn, E., Padin, X. A., Mercier, H., and Rios, A. F.: Temporal variability of the anthropogenic CO₂ storage in the Irminger Sea, *Biogeosciences*, 5, 1669–1679, doi:10.5194/bg-5-1669-2008, 2008.
- Pérez, F. F., Vázquez-Rodríguez, M., Mercier, H., Velo, A., Lherminier, P., and Ríos, A. F.: Trends of anthropogenic CO₂ storage in North Atlantic water masses, *Biogeosciences*, 7, 1789–1807, doi:10.5194/bg-7-1789-2010, 2010.
- Pérez, F. F., Mercier, H., Vázquez-Rodríguez M., Lherminier, P., Velo, A., Pardo, P. C., Rosón G., and Ríos A. F.: Atlantic Ocean CO₂ uptake reduced by weakening of the meridional overturning circulation, *Nat. Geosci.*, 6, 146–152, doi:10.1038/NGEO1680, 2013.
- Pickart, R. S., Straneo, F., and Moore, G. W. K.: Is Labrador Sea Water formed in the Irminger Basin?, *Deep-Sea Res. Pt. I*, 50, 23–52, 2003.
- Rhein, M., Fischer, J., Smethie Jr., W. M., Smythe-Wright, D., Weiss, R. F., Mertens, C., Min, D.-H., Fleischmann, U., and Putzka, A.: Labrador sea water: pathways, CFC-inventory and formation rates, *J. Phys. Oceanogr.*, 32, 648–665, 2002.
- Rhein, M., Kieke, D., Hüttl-Kabus, S., Roessler, A., Mertens, C., Meissner, R., Klein, B., Böning, C. W., and Yashayaev, I.: Deep water formation, the subpolar gyre, and the meridional overturning circulation in the subpolar North Atlantic, *Deep-Sea Res. Pt. II*, 58, 1819–1832, 2011.
- Rhein, M., Kieke, D., and Steinfeldt, R.: Ventilation of Upper Labrador Sea water, 2003–2005, *Geoph. Res. Lett.*, 34, L06603, doi:10.1029/2006GL028540, 2007.
- Roson, G., Rios, A. F., Lavin, A., Bryden, H. L., and Pérez, F. F.: Carbon distribution, fluxes and budgets in the subtropical North Atlantic, *J. Geophys. Res.*, 108, 3144, doi:10.1029/1999JC000047, 2003.
- Sabine, C. L., Feely, R. A., Gruber, N., Key, R. M., Lee, K., Bullister, J. L., Wanninkhof, R., Wong, C. S., Wallace, D. W. R., Tilbrook, B., Millero, F. J., Peng, T.-H., Kozyr, A., Ono, T., and Rios, A. F.: The oceanic sink for anthropogenic CO₂, *Science*, 305, 367–371, 2004.

Variability of the transport of anthropogenic CO₂ at the OVIDE section

P. Zunino et al.

Title Page

Abstract

Introduction

Conclusions

References

Tables

Figures

⏪

⏩

◀

▶

Back

Close

Full Screen / Esc

Printer-friendly Version

Interactive Discussion

- Sarafanov, A., Mercier, H., Falina, A., Sokov, A., and Lherminier, P.: Cessation and partial reversal of deep water freshening in the northern North Atlantic: observation-based estimates and attribution, *Tellus A*, 62, 80–90, 2010.
- Steinfeldt, R., Rhein, M., Bullister, J. L., and Tanhua, T.: Inventory changes in anthropogenic carbon from 1997–2003 in the Atlantic Ocean between 20° S and 65° N, *Global Biogeochem. Cy.*, 23, GB3010, doi:10.1029/2008GB003311, 2009.
- Straneo, F., Pickart, R. S., and Lavender, K.: Spreading of Labrador Sea water: an advective-diffusive study based on Lagrangian data, *Deep-Sea. Res. Pt. I*, 50, 701–719, doi:10.1016/S0967-0637(03)00057-8, 2003.
- Sy, A., Rhein, M., Lazier, J. R. N., Koltermann, K. P., Meincke, J., Putzka, A., and Bersch, M.: Surprisingly rapid spreading of newly formed intermediate waters across the North Atlantic Ocean, *Nature*, 386, 675–679, 1997.
- Tanhua, T., Biastoch, A., Körtzinger, A., Lüger, H., Böning, C., and Wallace, D. W. R.: Changes of anthropogenic CO₂ and CFC in the North Atlantic between 1981 and 2004, *Global Biogeochem. Cy.*, 20, GB4017, doi:10.1029/2006GB002695, 2006.
- Tjiputra, J. F., Assmann, K., and Heinze, C.: Anthropogenic carbon dynamics in the changing ocean, *Ocean Sci.*, 6, 605–614, doi:10.5194/os-6-605-2010, 2010.
- Våge K., Pickart, R., Thierry, V., Reverdin, G., Lee, C., Petrie, B., Agnew, T., Wong, A., and Ribergaard, M. H.: Surprising return of deep convection to the subpolar North Atlantic Ocean in winter 2007–2008, *Nat. Geosci.*, 2, 67–72, doi:10.1038/NCEO382, 2009.
- Vázquez-Rodríguez, M., Padin, X. A., Ríos, A. F., Bellerby, R. G. J., and Pérez, F. F.: An upgraded carbon-based method to estimate the anthropogenic fraction of dissolved CO₂ in the Atlantic Ocean, *Biogeosciences Discuss.*, 6, 4527–4571, doi:10.5194/bgd-6-4527-2009, 2009.
- Velo, A., Pérez, F. F., Lin, X., Key, R. M., Tanhua, T., de la Paz, M., Olsen, A., van Heuven, S., Jutterström, S., and Ríos, A. F.: CARINA data synthesis project: pH data scale unification and cruise adjustments, *Earth Syst. Sci. Data*, 2, 133–155, doi:10.5194/essd-2-133-2010, 2010.
- Yashayaev, I. and Loder, J. W.: Enhanced production of Labrador Sea water in 2008, *Geoph. Res. Lett.*, 36, L01606, doi:10.1029/2008GL036162, 2009.
- Yashayaev, I., van Aken, H. M., Holliday, N. P., and Bersch, M.: Transformation of the Labrador Sea water in the subpolar North Atlantic, *Geoph. Res. Lett.*, 34, L22605, doi:10.1029/2007GL031812, 2007

Variability of the transport of anthropogenic CO₂ at the OVIDE section

P. Zunino et al.

Table 1. Estimations of transport of Cant (T_{Cant}) in the North Atlantic from the literature. The T_{Cant} is often given in PgCyr⁻¹ (1 PgCyr⁻¹ = 2642 kmols⁻¹).

Reference	Latitude	Time	Method	T_{Cant} (kmols ⁻¹)
Mikaloff Fletcher et al. (2006)	18° N	1765–1995	ocean inversion	317 ± 26
Gruber et al. (2009)	24.5° N	1765–1995	ocean inversion	211
Tjiputra et al. (2010)	24.5° N	1990s–2000s	biogeochemical model	396 ± 106
Roson et al. (2003)	24.5° N	1992	observations	634 ± 211
Macdonald et al. (2003)	24.5° N	1992–1998	observations	502 ± 211
Pérez et al. (2013)	40–60° N	2002–2006 (referred to 2004)	observations	195 ± 24
Mikaloff Fletcher et al. (2006)	49° N	1765–1995	ocean inversion	53 ± 26
Tjiputra et al. (2010)	49° N	1990s–2000s	biogeochemical model	~ 100

Title Page

Abstract

Introduction

Conclusions

References

Tables

Figures

⏪

⏩

◀

▶

Back

Close

Full Screen / Esc

Printer-friendly Version

Interactive Discussion

Variability of the transport of anthropogenic CO₂ at the OVIDE section

P. Zunino et al.

[Title Page](#)

[Abstract](#)

[Introduction](#)

[Conclusions](#)

[References](#)

[Tables](#)

[Figures](#)



[Back](#)

[Close](#)

[Full Screen / Esc](#)

[Printer-friendly Version](#)

[Interactive Discussion](#)

Table 2. Hydrographic cruises.

Cruise name	Month/year	Vessel	Reference
FOUREX 1997	08–09/1997	R/V <i>Discovery</i>	Alvarez et al. (2002)
OVIDE 2002	06–07/2002	N/O <i>Thalassa</i>	Lherminier et al. (2007)
OVIDE 2004	06–07/2004	N/O <i>Thalassa</i>	Lherminier et al. (2010)
OVIDE 2006	05–06/2006	R/V <i>Maria S. Merian</i>	Gourcuff et al. (2011)
OVIDE 2008	06–07/2008	N/O <i>Thalassa</i>	Mercier et al. (2013)
OVIDE 2010	06–07/2010	N/O <i>Thalassa</i>	Mercier et al. (2013)

Variability of the transport of anthropogenic CO₂ at the OVIDE section

P. Zunino et al.

Title Page

Abstract

Introduction

Conclusions

References

Tables

Figures



Back

Close

Full Screen / Esc

Printer-friendly Version

Interactive Discussion

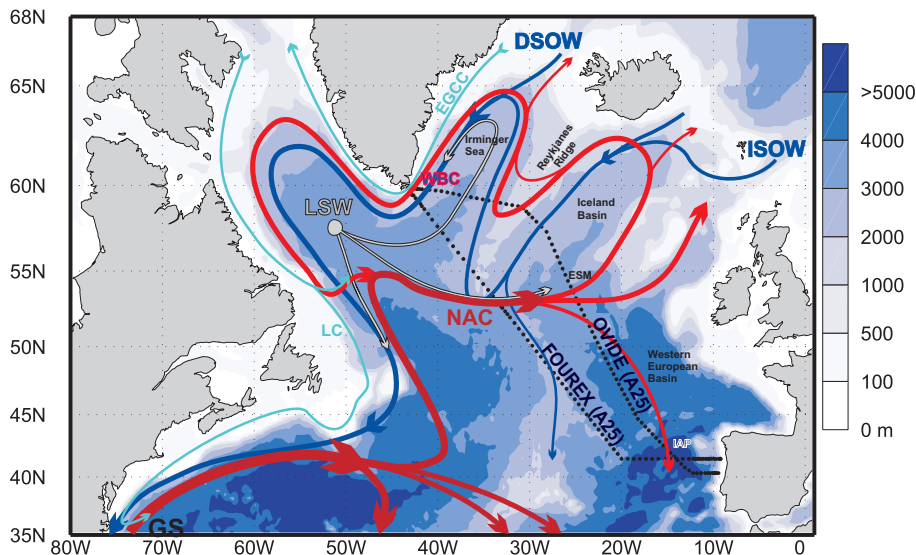


Fig. 1. Schematic circulation in the North Atlantic. The main pathways of warm and salty waters originating from the subtropical Atlantic Ocean are shown in red lines while the deep currents are displayed in dark blue. The cyan lines represent the fresh and cold currents over the shelves (Eastern Greenland Coastal Current (EGCC) and Labrador Current (LC)). The grey lines indicate the spreading of the Labrador Sea Water (LSW). OVIDE and FOUREX sections are represented with dotted lines. The background displays the bathymetry. The other abbreviations stand for: DSOW = Demark Strait Overflow Water, ISOW = Iceland Scotland Overflow Water, WBC = Western Boundary Current, NAC = North Atlantic Current, GS = Gulf Stream, ESM = Eriador Seamount, IAP = Iberian Abyssal Plain.

Variability of the transport of anthropogenic CO₂ at the OVIDE section

P. Zunino et al.

Title Page

Abstract

Introduction

Conclusions

References

Tables

Figures



Back

Close

Full Screen / Esc

Printer-friendly Version

Interactive Discussion

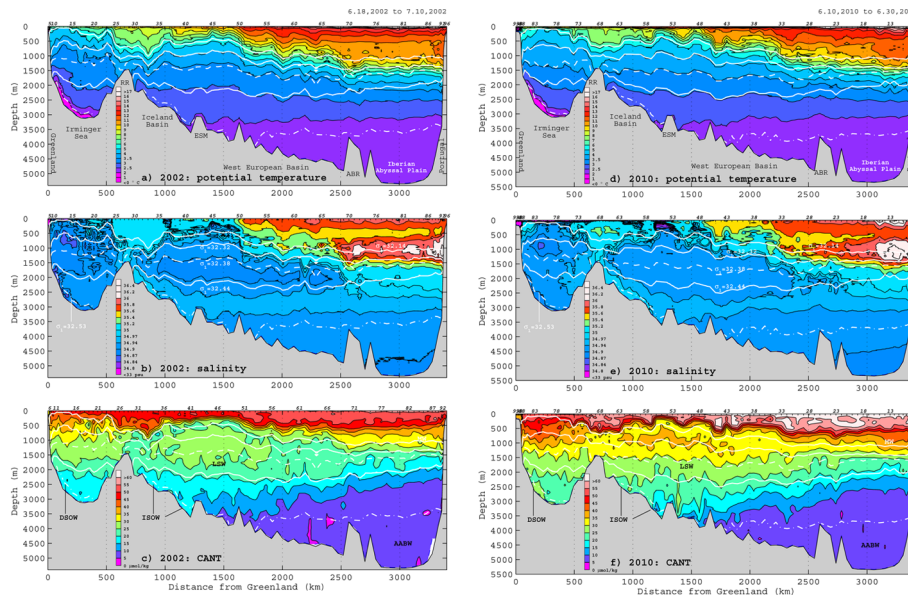


Fig. 2. OVIDE sections of 2002 and 2010 of **(a, d)** potential temperature in °C, **(b, e)** salinity and **(c, f)** anthropogenic carbon dioxide in $\mu\text{mol kg}^{-1}$. The depth of the isopycnals referenced in the manuscript are plotted in all the figures, their specific values are indicated in **(b)** and **(e)**. All the water masses cited in the manuscript are localized in the section in **(c)** and **(f)**: DSOW = Demarc Strait Overflow Water, ISOW = Iceland Scotland Overflow Water, LSW = Labrador Sea Water, MW = Mediterranean Water, AABW = Antarctic Bottom Water. The other abbreviations in **(a)** and **(d)** stand for: RR = Reykjanes Ridge, ESM = Eriador Sea Mount and ABR = Azores–Biscay Ridge. The numbers on the top of each plot indicate the station numbers corresponding to each survey.

Variability of the transport of anthropogenic CO₂ at the OVIDE section

P. Zunino et al.

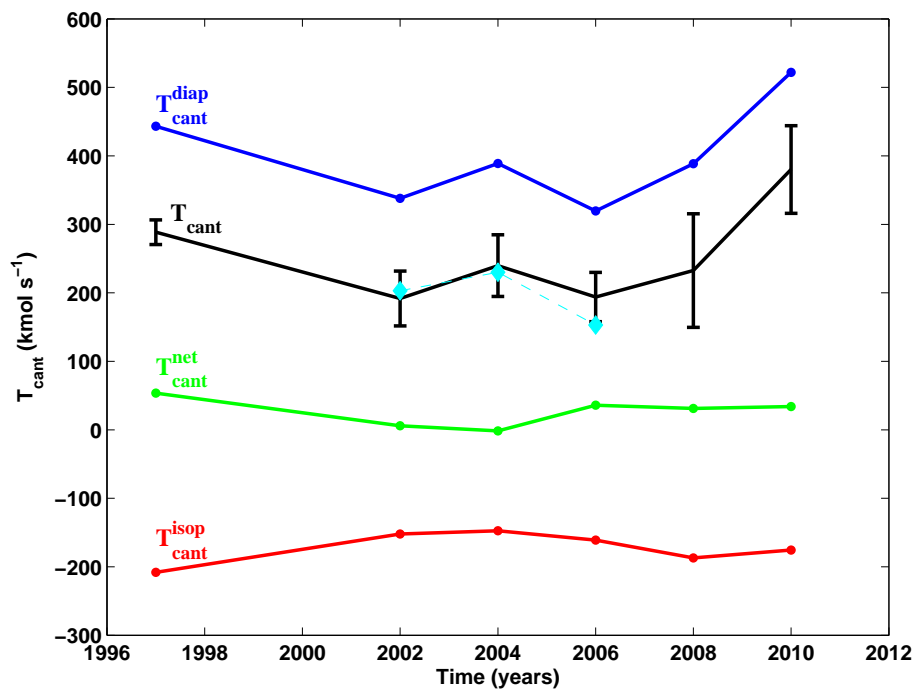


Fig. 3. T_{Cant} (black) and its components (blue, red and green) across the OVIDE section as a function of time. The cyan diamonds are the T_{Cant} computed by Pérez et al. (2013); for that computation they referenced Cant data to the year 2004.

[Title Page](#)
[Abstract](#)
[Introduction](#)
[Conclusions](#)
[References](#)
[Tables](#)
[Figures](#)
[◀](#)
[▶](#)
[◀](#)
[▶](#)
[Back](#)
[Close](#)
[Full Screen / Esc](#)
[Printer-friendly Version](#)
[Interactive Discussion](#)

Variability of the transport of anthropogenic CO₂ at the OVIDE section

P. Zunino et al.

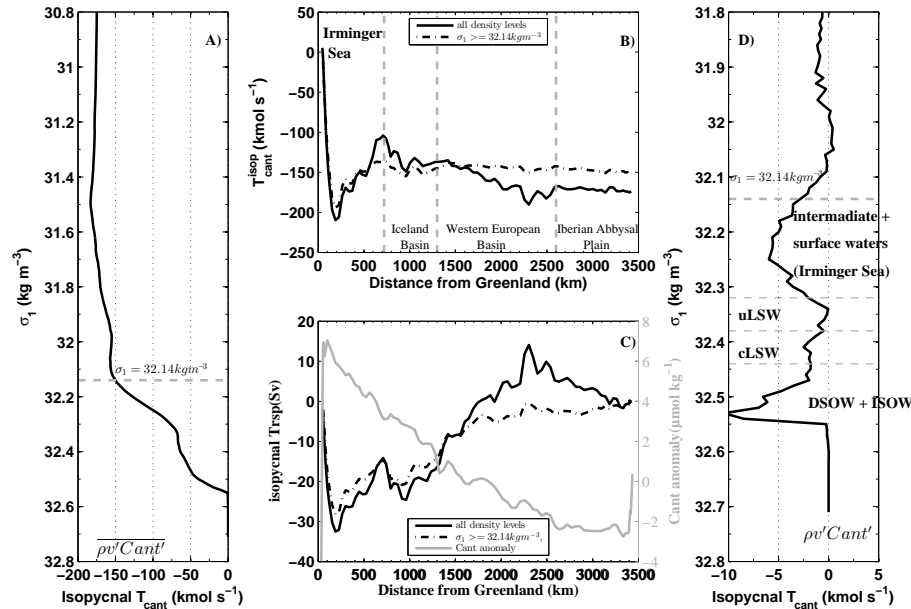


Fig. 4. Transport of Cant caused by the isopycnal component (T_{Cant}^{isop}) averaged over time. **(A)** T_{Cant}^{isop} accumulated from the bottom to each specific density level. **(B)** T_{Cant}^{isop} horizontally accumulated from Greenland to each station along the section, and vertically integrated for the whole column of water (continuous lines) and for waters denser than 32.14 kg m^{-3} (dashed lines). **(C)** On the left axis: isopycnal volume transport accumulated from Greenland to each station, and vertically integrated for the whole column of water (continuous black line) and for waters denser than 32.14 kg m^{-3} (dashed black lines). On the right axis, in grey, mean value of Cant anomalies vertically averaged all along the section. **(D)** T_{Cant}^{isop} horizontally but not vertically integrated (see Fig. 1 for the abbreviations). Note that in plots **(A)** and **(D)**, the vertical axes do not have the same scales.

Title Page

Abstract

Introduction

Conclusions

References

Tables

Figures

◀

▶

◀

▶

Back

Close

Full Screen / Esc

Printer-friendly Version

Interactive Discussion

Variability of the transport of anthropogenic CO₂ at the OVIDE section

P. Zunino et al.

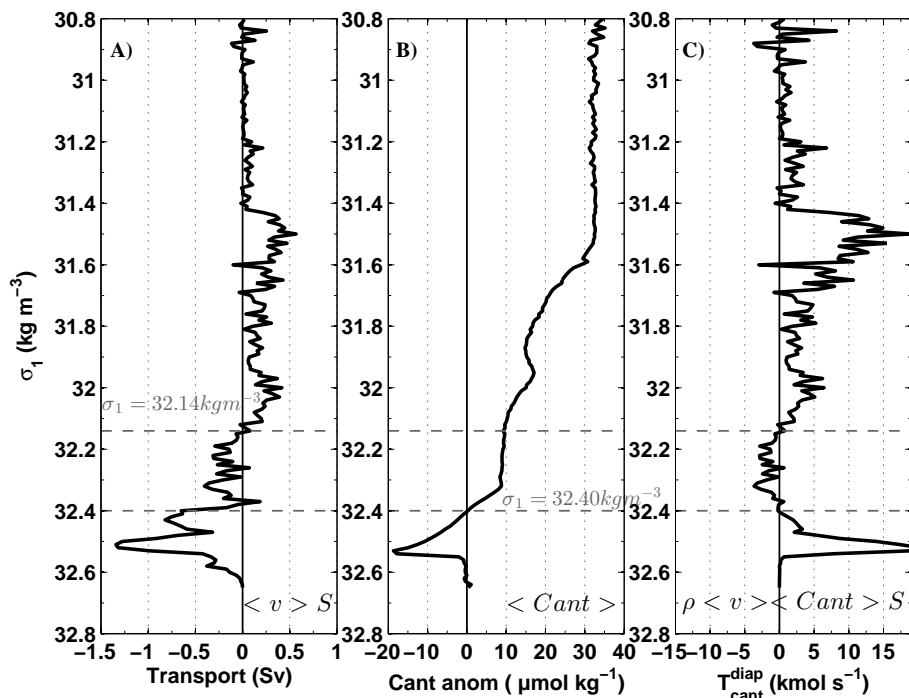


Fig. 5. T_{Cant}^{diap} and the different elements by which it was computed. **(A)** Volume transport integrated in density (σ_1) layers with a 0.01 kg m^{-3} resolution. **(B)** Mean profile of anomaly of Cant averaged at each density layer, this anomaly in relation to the section-average value. **(C)** T_{Cant}^{diap} profile. All the data represented in this figure are the averages of the six surveys analyzed in this work.

Title Page

Abstract Introduction

Conclusions References

Tables Figures

⏪ ⏩

◀ ▶

Back Close

Full Screen / Esc

Printer-friendly Version

Interactive Discussion



Variability of the transport of anthropogenic CO₂ at the OVIDE section

P. Zunino et al.

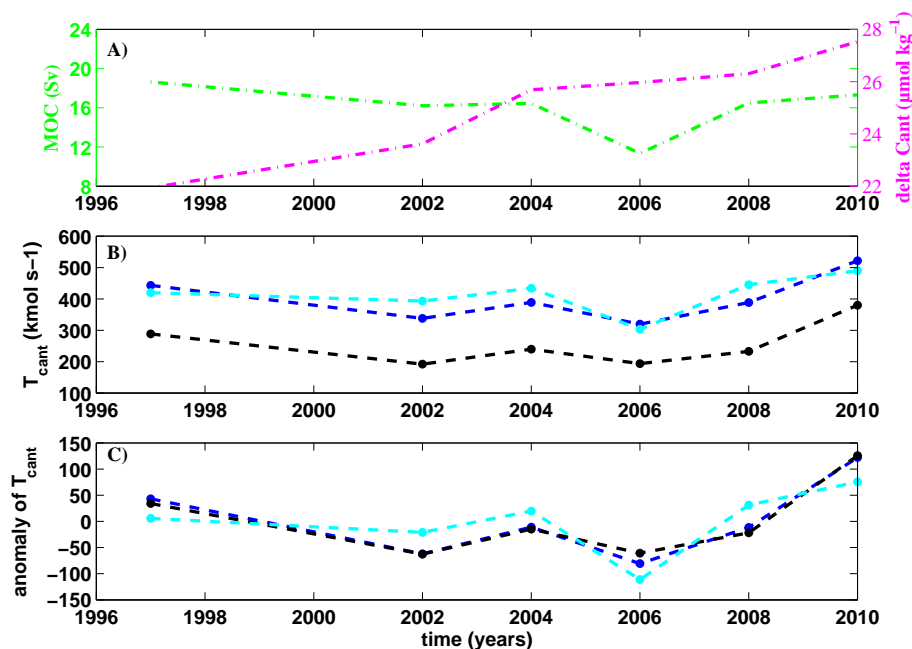


Fig. 6. (A) Time evolution of the intensity of the MOC (MOC_{σ} in green) and of the difference of Cant between the upper and lower limbs of the MOC (in pink). (B) Time evolution of T_{Cant} (black line), $T_{\text{Cant}}^{\text{diap}}$ (blue line) and T_{Cant} computed by the estimator (T_{Cant}° , cyan line). (C) Time evolution of anomalies of T_{Cant} (black line), $T_{\text{Cant}}^{\text{diap}}$ (blue line), T_{Cant}° (cyan line), the anomalies in relation to the mean value computed over 1997–2010.

[Title Page](#)
[Abstract](#)
[Introduction](#)
[Conclusions](#)
[References](#)
[Tables](#)
[Figures](#)
[Back](#)
[Close](#)
[Full Screen / Esc](#)
[Printer-friendly Version](#)
[Interactive Discussion](#)

Variability of the transport of anthropogenic CO₂ at the OVIDE section

P. Zunino et al.

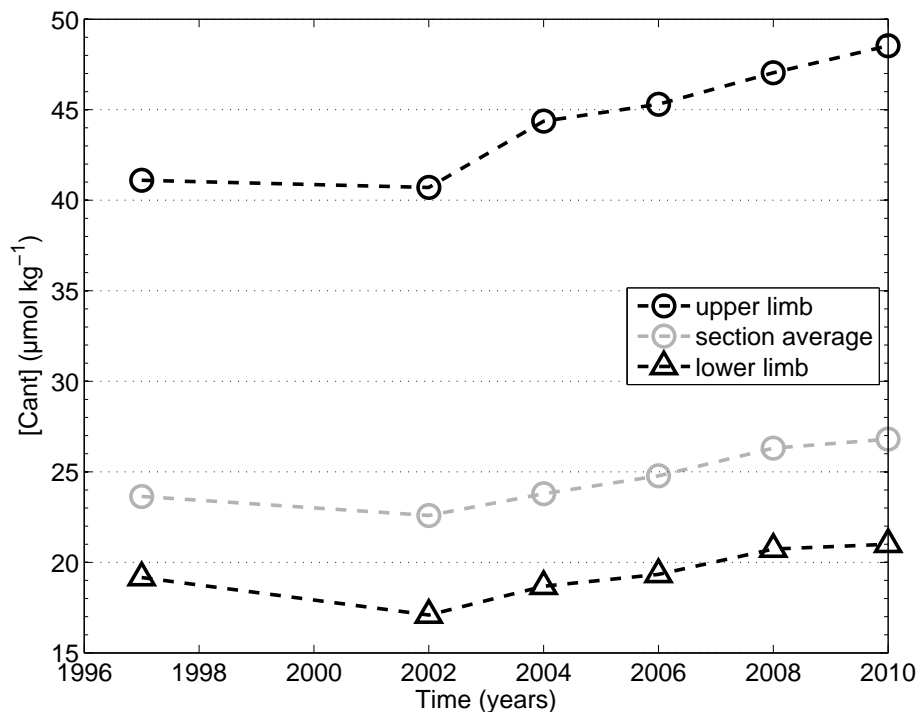


Fig. 7. Time evolution of Cant concentrations: upper limb of the MOC (empty black circles) section average value (empty grey circles), and lower limb of the MOC (empty black triangles).

[Title Page](#)[Abstract](#)[Introduction](#)[Conclusions](#)[References](#)[Tables](#)[Figures](#)[◀](#)[▶](#)[◀](#)[▶](#)[Back](#)[Close](#)[Full Screen / Esc](#)[Printer-friendly Version](#)[Interactive Discussion](#)